

# Study of 2D interpolating readout for a micro-pattern gaseous detector

DONG Ming-Yi(董明义)<sup>1,2</sup> XIU Qing-Lei(修青磊)<sup>1,2,3</sup> LIU Rong-Guang(刘荣光)<sup>1,2</sup>  
 ZHANG Jian(张建)<sup>1,2</sup> OUYANG Qun(欧阳群)<sup>1,2</sup> CHEN Yuan-Bo(陈元柏)<sup>1,2</sup>

<sup>1</sup> State Key Laboratory of Particle Detection and Electronics, Beijing 100049, China

<sup>2</sup> Institute of High Energy Physics, Chinese Academy of Sciences, Beijing 100049, China

<sup>3</sup> Graduate University of Chinese Academy of Sciences, Beijing 100049, China

**Abstract:** The two-dimensional interpolating readout, a new readout concept based on resistive anode structure, was studied for the micro-pattern gaseous detector. Within its high spatial resolution, the interpolating resistive readout structure leads to an enormous reduction of electronic channels compared with pure pixel devices, and also makes the detector more reliable and robust, which is attributed to its resistive anode relieving discharge. A GEM (gaseous electron multiplier) detector with 2D interpolating resistive readout structure was set up and the performance of the detector was studied with <sup>55</sup>Fe 5.9 keV X-ray. The detector worked stably at the gain up to  $3.5 \times 10^4$  without any discharge. An energy resolution of about 19%, and a spatial resolution of about 219  $\mu\text{m}$  (FWHM) were reached, and good imaging performance was also obtained.

**Key words:** interpolating readout, resistive anode readout structure, micro-pattern gaseous detector, GEM

**PACS:** 29.40.Cs, 29.40.Gx **DOI:** 10.1088/1674-1137/37/2/026002

## 1 Introduction

Micro-pattern gaseous detectors such as the GEM [1], the thick GEM [2] and the MICROMEGAS (micro mesh gaseous structure) [3] have been the subject of numerous studies and been suitable candidates for particle physics experiments and X-ray imaging experiments like small angle scattering or protein crystallography at synchrotron light sources, because they have attractive features of high gas gain of  $10^3$ – $10^4$ , sufficient energy resolution, suitable imaging performance in combination with an adequate readout structure. But a large number of readout channels are required in the case of the application demanding high spatial resolution, and the detectors do not work stably due to the discharge at high gas gains. So two-dimensional interpolating readout, a new readout concept based on resistive anode structure, was developed by H. J. Besch in 1997 [4], which can be applied to any micro-pattern gaseous detectors described above. Further research on this resistive readout structure employed in a CAT detector were performed by H. J. Besch group at Siegen, Germany [5–7]. Within its count rate capability, the interpolating resistive readout structure permits the performance of a pure pixel detector with a spatial resolution of about 200  $\mu\text{m}$  to be reached with the number of electronic readout channels needed per area being reduced by two orders of magnitude, and

at the same time, the resistive anode can relieve the discharge and make the detector reliable and robust at high gains.

In order to understand the physical behavior of this two-dimensional interpolating structure and to optimize this device for applications, resistive anode readout structures based on ceramics were manufactured and applied to a GEM detector, and the performance of the detector was studied with <sup>55</sup>Fe 5.9 keV X-ray.

## 2 The detector setup and working principle

In our detector development, triple GEM foils were chosen as the gas gain device with resistive readout anode structure. Fig. 1 shows a schematic diagram of the detector setup. Primary electrons generated in the gas conversion region by incoming photons via photoelectric effect are led by a homogeneous electric drift field towards the gas gain region, the triple GEM structure, where they are multiplied in an avalanche process. Then the charge cluster hits the readout plane, designed as a two-dimensional interpolating resistive structure, where the sensitive area is subdivided into  $6 \times 6$  square, 8 mm  $\times$  8 mm sized cells. Each cell (as shown in Fig. 2), which has an edge length of  $g=8$  mm and a surface resistance of 1000  $\text{k}\Omega/\square$ , is surrounded by better conducting borders with a width

Received 21 March 2012, Revised 23 April 2012

©2013 Chinese Physical Society and the Institute of High Energy Physics of the Chinese Academy of Sciences and the Institute of Modern Physics of the Chinese Academy of Sciences and IOP Publishing Ltd

of about 200  $\mu\text{m}$  and a surface resistance of 10  $\text{k}\Omega/\square$ . The resistive material is printed onto ceramics, and these two different surface resistivities are used to obtain both an almost linear charge division behavior in both  $x$ - and  $y$ - direction and a good electrical shielding which avoids excessively large charge distributions over several cells.

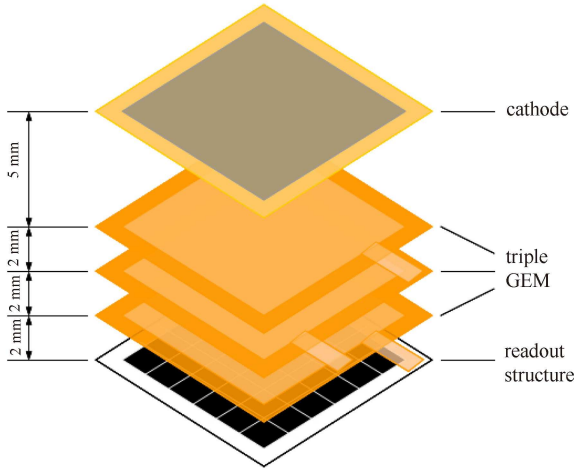


Fig. 1. Schematic cross section of the triple-GEM detector set-up with the 2D interpolating resistive readout structure.

The charges flow to the low input impedance readout nodes at the four corners of the cells, which are connected by small connections to the back of the resistive readout structure and then to the charge-sensitive preamplifiers. The analogue signals from the charge-sensitive preamplifiers are directly converted to digital signals by a 12-bit peak ADC which is linked to a dedicated DAQ system through CAMAC bus, and the signal from the bottom of the undermost GEM is used for the readout trigger (as shown in Fig. 3). The DAQ system pre-processes the

data for the online visualization and saves the raw data in a local hard disk for the offline analysis.

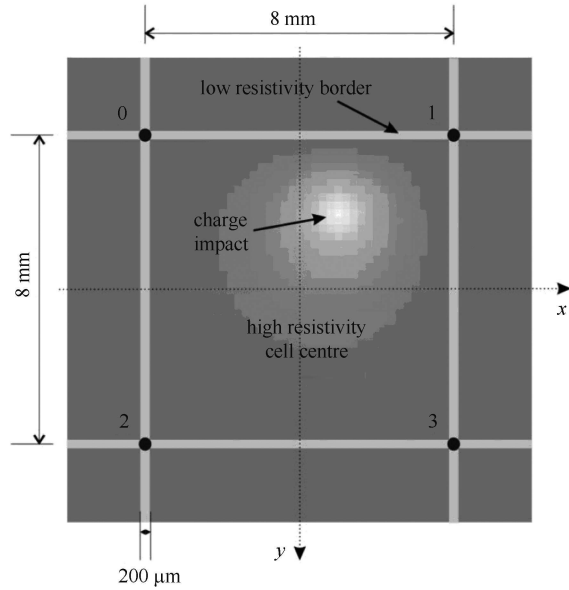


Fig. 2. Schematic of one cell of the resistive readout structure for micro-pattern gaseous detectors.

By means of suitable algorithms, e.g. linear reconstruction algorithms, and using the collected charges  $Q_i$  at the four readout nodes of an impacted cell (the so-called four-node-encoding algorithm), the event position can be calculated within the cell.

Each electrode of the detector is in a tight box flowing with  $\text{Ar}/\text{CO}_2$  (70:30) operation gas at atmospheric pressure, and the conversion region, transfer regions and induction region thicknesses of the detector are 5 mm, 2 mm, 2 mm and 2 mm respectively.

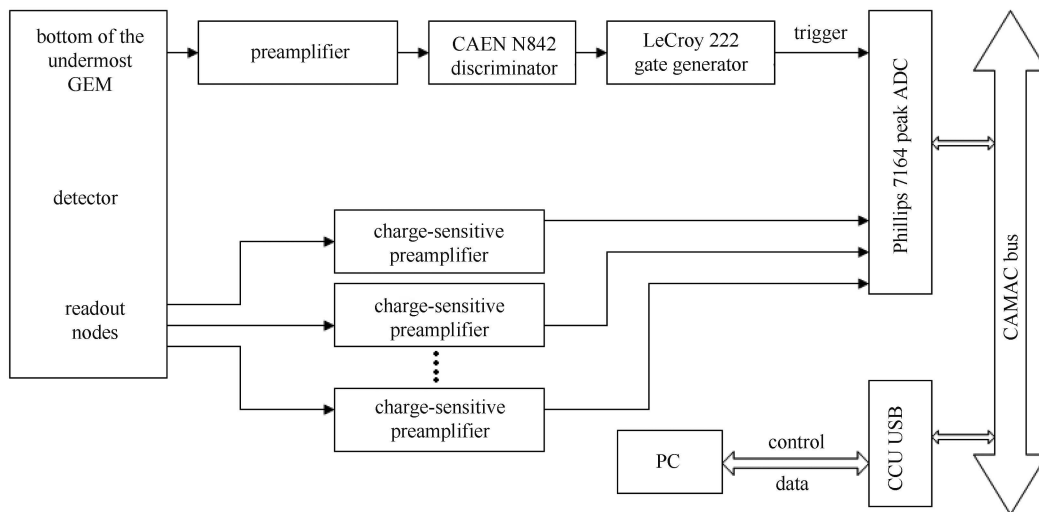


Fig. 3. Block schematic of the readout.

### 3 The detector performance

Using a single readout cell, we have studied the performance of the GEM detector with the interpolating resistive readout structure, and the linear position reconstruction algorithm.

#### 3.1 The gas gain

The effective gas gain of the GEM detector as a function of the multipliable high voltage across the triple GEM electrodes  $\Delta V_{\text{GEM}}$  ( $\Delta V_{\text{GEM1}} + \Delta V_{\text{GEM2}} + \Delta V_{\text{GEM3}}$ ) and the electric field strength of induction  $E_I$  have been studied. In the test,  $^{55}\text{Fe}$  5.9 keV X-rays were collimated on the resistive readout cell by an aluminum collimator with a small hole.

Figure 4(a) shows the effective gain of the detector as a function of  $\Delta V_{\text{GEM}}$ , with drift electric field  $E_D = 2$  kV/cm and induction electric field  $E_I = 2$  kV/cm. The effective gain of the detector increases with  $\Delta V_{\text{GEM}}$  by a good exponential way. When  $\Delta V_{\text{GEM}}$  is up to 1220 V, the effective gain of the detector can reach  $3.5 \times 10^4$ .

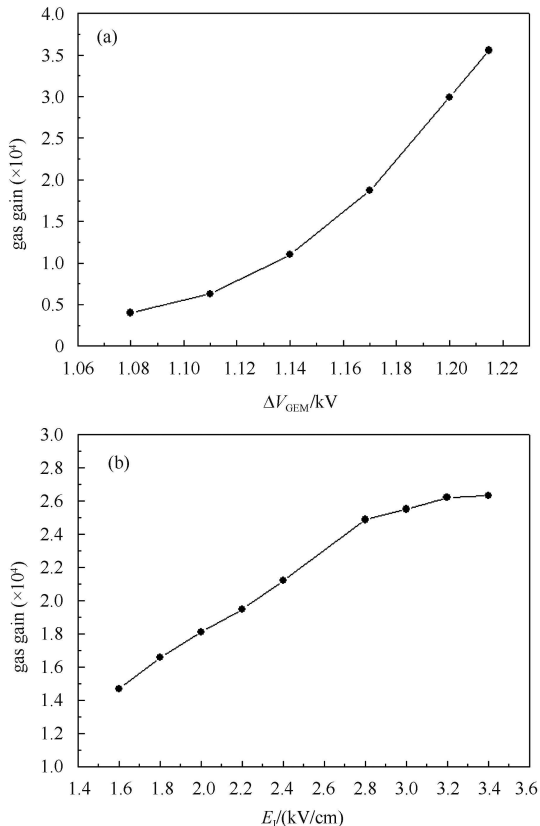


Fig. 4. (a) The effective gain as a function of multipliable high voltage across the triple GEM electrodes  $\Delta V_{\text{GEM}}$ , and (b) the effective gain as a function of induction electric field  $E_I$ .

Figure 4(b) shows the effective gain of the detector as a function of  $E_I$ , with  $E_D = 2$  kV/cm and  $\Delta V_{\text{GEM}} = 1170$  V. The result shows that the effective gain of the detector can reach a saturation state and the avalanched electrons are almost fully collected by the resistive readout anode, when the electric field in the induction region is over 2.8 kV/cm.

#### 3.2 The stability

The stability of the detector was studied at the effective gas gain of about  $3.5 \times 10^4$ . Over 24 hours, the effective gas gain was tested every 7 minutes. The detector had no discharge and the variance of gas gain was about 3% in the whole test, which indicated that with the resistive readout structure, the detector was robust and could work stably at high gains.

#### 3.3 The energy resolution and linearity

The energy resolution of the GEM detector with resistive readout structure was measured with  $^{55}\text{Fe}$  5.9 keV X-ray collimated by 10 mm thick aluminum with a 500  $\mu\text{m}$  slit. Because the charges on the resistive readout anode were collected by the 4 readout nodes of one cell through charge division, we summed up the 4 signals to obtain the 5.9 keV X-ray full energy spectrum.

Figure 5 shows the energy spectrum of  $^{55}\text{Fe}$  with  $E_D = 2$  kV/cm,  $\Delta V_{\text{GEM}} = 1170$  V and  $E_I = 2$  kV/cm, and the detector was operated at an effective gain of about  $2 \times 10^4$ . The energy resolution of the  $^{55}\text{Fe}$  5.9 keV X-ray full energy photo-electron peak is 19% (FWHM), and the escape peak of Ar atoms is obvious. The ratio of 5.9 keV X-ray peak and escape peak is about 1.92, which means that the detector system has good energy linearity.

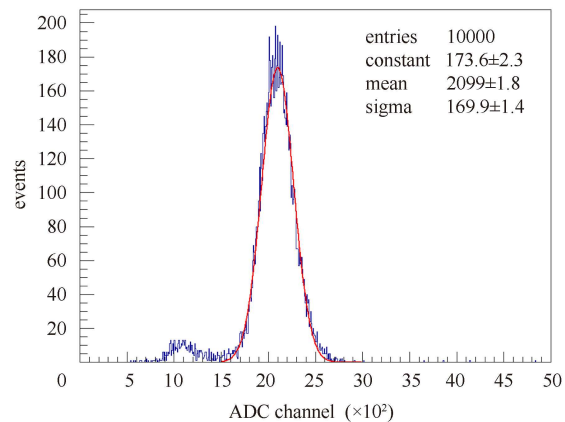


Fig. 5. The energy resolution of the detector with  $^{55}\text{Fe}$  5.9 keV X-ray.

#### 3.4 The spatial resolution

The spatial resolution was measured with  $^{55}\text{Fe}$  5.9 keV X-ray collimated by 10 mm thick aluminum with a 500  $\mu\text{m}$  slit.

Using the collected charges  $Q_i$  at the four readout nodes of one cell, the impact position of a photon is reconstructed with linear four-node-encoding algorithm described by Eq. (1).

$$x = \frac{g}{2} \frac{(Q_1 + Q_3) - (Q_0 + Q_2)}{Q_0 + Q_1 + Q_2 + Q_3}$$

and

$$y = \frac{g}{2} \frac{(Q_2 + Q_3) - (Q_0 + Q_1)}{Q_0 + Q_1 + Q_2 + Q_3}, \quad (1)$$

where  $g$  is the cell length, and  $Q_0, Q_1, Q_2, Q_3$  are the signals from the four nodes surrounding a cell counting clockwise from the upper left corner as shown in Fig. 2. For events in the central area of a cell the applied algorithm derives the correct center of gravity. However, for border events a small fraction of the charge is deposited on neighboring cells, thus partially losing signal information. Consequently, the position of an event is shifted towards the cell center causing the depleted cell borders in the measured image. These distortions, which are dominated by diffusion, can be reduced by using short gas depths, high drift fields and low diffusion gas mixtures, and also can be corrected with three-node algorithm, six-node algorithm and non-linear position reconstruction algorithms. These reconstruction algorithms, which require use of the information of the charges collected by the neighbor cells, are under study.

Figure 6 shows that the spatial resolution of the detector reaches about 219  $\mu\text{m}$  ( $\text{FWHM} = 2.355\sigma$ ) with convolution fit methods [8] which can take out the influence of the collimation slit on the position accuracy. The result can be comparable to the pure pixel detector with

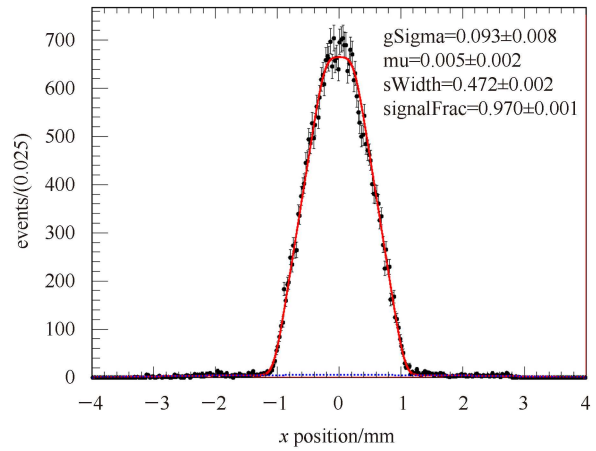


Fig. 6. The spatial resolution of the detector with convolution fit.

pixel size of about 0.3 mm×0.3 mm.

### 3.5 The imaging performance

The imaging performance was studied by placing a mask between the  $^{55}\text{Fe}$  source and incidence window of the detector. The mask was made up of a 30 mm thick aluminum plate with a hole of the character “L”, and the width of the “L” shape slit was 500  $\mu\text{m}$ .

The impact position was reconstructed also by linear four-node-encoding algorithm described by Eq. (1), and a two-dimensional image, shown in Fig. 7, was obtained, which is good enough for the border of the “L” to be clear. The result illustrates that the detector has a good image performance and good uniformity of response.

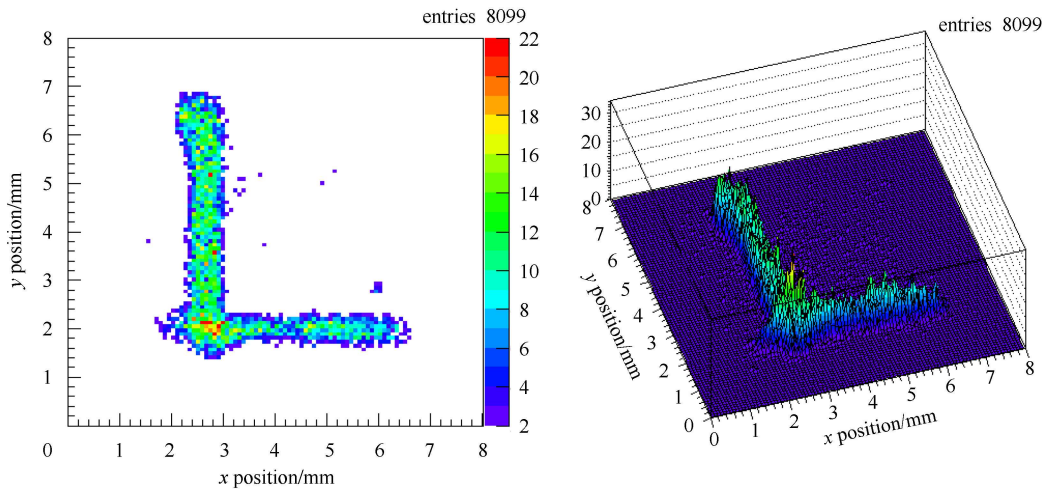


Fig. 7. The imaging of the detector with  $^{55}\text{Fe}$  5.9 keV X-ray.

## 4 Conclusion and discussion

The interpolating resistive readout system presented here provides a good spatial resolution of 219  $\mu\text{m}$  (FWHM) and a sufficient imaging performance even with simple linear algorithms. It is expected that after a further reduction of the diffusion in the gas and an optimization of the resistances of the anode readout structure and with non-linear position reconstruction algorithms and correction functions, a much better spatial resolution and imaging performance can be achieved, which would be an important advantage for the future two-dimensional position-sensitive X-ray detector.

Compared with the conventional strip readout method, the interpolating resistive anode readout method is truly two-dimensional, which is an essential requirement for obtaining a high global rate capability

for large-scale devices. In contrast to a pure pixel detector, the number of electronic channels needed per area is tremendously reduced, thus offering a more cost effective system.

The resistive anode readout structure also reduces the probability of the discharge which can contribute to the stability of the detector. So the detector can work stably with the operation multipliable voltage  $\Delta V_{\text{GEM}}$  up to 1220 V at which the relative gain is up to  $3.5 \times 10^4$ .

From the test results of the performance of the interpolating resistive anode readout structure, we expect that this readout structure has a potential application in micro-pattern gaseous detectors.

*We wish to express our thanks to Prof. Li Ren-ying for providing a charge-sensitive preamplifier, as well as to Prof. Xie Yi-gang and Dr. Lv-Xinyu for their useful suggestions and discussions.*

---

## References

- 1 Sauli F. Nucl. Instrum. Methods A, 1997, **386**(2-3): 531
- 2 Chechik R, Breskin A, Shalem C et al. Nucl. Instrum. Methods A, 2004, **535**(1-2): 303
- 3 Giomataris Y, Rebourgeard Ph, Robert J P et al. Nucl. Instrum. Methods A, 1996, **376**(1): 29
- 4 Besch H J, Junk M, Meißner W et al. Nucl. Instrum. Methods A, 1997, **392**(1-3): 244
- 5 Sarvestani A, Besch H J, Junk M et al. Nucl. Instrum. Methods A, 1998, **419**(2-3): 444
- 6 Orthen A, Wagner H, Besch H J et al. Nucl. Instrum. Methods A, 2002, **478**(1-2): 200
- 7 Wagner H, Besch H J, Menk R H et al. Nucl. Instrum. Methods A, 2002, **482**(1-2): 334
- 8 LÜ Xin-Yu, FAN Rui-Rui, CHEN Yuan-Bo et al. CPC (HEP & NP), 2012, **36**(3): 228